Tiara-like Complexes acting as Iodine Encapsulating Agents: The Role of M I Interactions in [M(μ-SCH2CO2Me)2]8⊂I2 (M = Ni, Pd, Pt) Inclusion Compounds

Miguel-Armando Ponce-Vargas, Alvaro Munoz-Castro

Tiara-like Complexes acting as Iodine Encapsulating Agents. The Role of M···I Interactions in $[M(\mu\text{-}SCH_2CO_2Me)_2]_8 \subset I_2$ (M=Ni, Pd, Pt) Inclusion Compounds

Miguel Ponce-Vargas[a*], *Alvaro Muñoz-Castro*[b*]

[a] Institut des Sciences Chimiques de Rennes, UMR 6226 CNRS-Université de Rennes 1, 263 Avenue du Général Leclerc, 35042 Rennes Cedex, France.
E-mail: miguel-armando.ponce-vargas@univ-rennes1.fr
Phone: +33 (0) 2.23.23.69.73

[b] Grupo de Química Inorgánica y Materiales Moleculares, Universidad Autónoma de Chile, El Llano Subercaseaux 2801, Santiago, Chile.
E-mail: alvaro.munoz@uautonoma.cl

ABSTRACT

A proposed series of tiara-like complexes $[M(\mu\text{-}SCH_2CO_2Me)_2]_8$ (where M = Ni, Pd, Pt) are here studied through DFT methodologies prompted by the synthesis of the palladium parent and their potential application in iodine encapsulation from spent nuclear fuel. Their hollow structure with a suitable cavity size, and the presence of several transition-metal centers capable to directly interact with an I_2 molecule through noncovalent

forces, make them attractive inclusion agents. Herein, an Energy Decomposition Analysis reveals that forces responsible for keeping the guest molecule in the inner cavity are mainly electrostatic; a remarkable feature given, in principle, the neutral nature of both the host and guest species, offering us an interesting study case where the electronic cloud distortion of the binding sites and iodine atoms can be estimated and related to the intensity of the host-guest interactions. Our results shed light into the application of the nickel tiara-like host as an alternative to the reported $[Pd(\mu\text{-}SCH_2CO_2Me)_2]_8$ system. This research can be useful for further evaluation of nickel-based iodine sequestering agents prior to engaging in explorative synthesis efforts.

INTRODUCTION

The effective capture and storage of radioiodine is of paramount importance in public safety given its high mobility and the long half-life of the ^{129}I isotope[1,2]. Therefore, the development of different approaches towards the encapsulation of I_2 has become the primary goal of multiple research teams devoted to materials sciences[3,4]. Nowadays, the strategy to capture I_2 released from nuclear exhaust gas usually involves the iodine precipitation in solution by using porous solids including zeolites[2,5,6], coordination polymers[7], hybrid porous materials[8,9], nanocomposites[10], and metal-containing systems[11]. In this last group, metallacycles appear as promising candidates due to the vast number of hollow geometries they are able to offer[12,13,14], allowing different size cavities suitable for iodine. Moreover, the presence of metal centers capable of interacting with the iodine molecule through noncovalent forces represents a clear advantage over their pure organic counterparts. The host-guest capabilities of metallacycles have been already demonstrated, in particular towards small molecules[15] and anions[16]. With respect to extended metal-containing systems, in addition to the widely used silver-containing mordenites[1], other effective I_2 inclusion materials such as Zn(II)-metal-organic frameworks[17], Zn(II)-coordination polymers[9] and supramolecular networks constructed by one-dimensional $M[(ebic)_2]_n$ linear chains (where M = Zn, Co and Hebic = 2-ethyl-1*H*-benzo[d]imidazole-5-carboxylic acid)[18] have been hitherto reported.

The rationalization of the forces established between metal-containing systems and halogens is a current subject of research with the aim of obtaining novel iodine sequestering agents. In this regard, the intensity of noncovalent interactions can be related to the electronic cloud distortion experienced by the binding sites, i.e. the metal

centers, in order to gain a deeper understanding of the forces governing the iodine encapsulation. Similar studies related to halogen bonding[19,20], amino acids dimers[21], *S*-heterocycles-diiodine complexes[22], and water molecules[23,24] have been conducted, where an explanation of the noncovalent forces supported on electronic cloud distortions in terms of multipoles, is proposed.

Following our interest in metallacycle host-guest capabilities[25,26], here we study through density functional theory (DFT) methodologies a series of tiara-like octanuclear complexes $[M(\mu\text{-}SCH_2CO_2Me)_2]_8$ (where M = Ni, Pd, Pt) and their corresponding iodine inclusion compounds. The palladium and platinum systems have been recently synthesized by Ura and coworkers[14,27]. It is the formally neutral character of the tiara-like metal containing complex and the iodine guest that prompts us to study these inclusion compounds, where the electronic cloud distortion of the binding sites and iodine atoms leading to multipole-multipole forces is to a large extent responsible for keeping the guest in the host cavity. To conduct this research we employ a noncovalent interactions analysis (NCI)[28,29] in order to identify the binding sites; an Energy Decomposition Analysis (EDA)[30,31] to clarify the nature of the noncovalent forces; a Natural Population Analysis (NPA)[32] to determine if a significant charge transfer between the host and the guest occurs; and a Multipole Analysis[33] to estimate the electronic cloud deviations occurring at the binding sites with the iodine incorporation. Additionally, DFT calculations were also performed on simplified models with methyl groups and hydrogen atoms instead of the methoxycarbonylmethyl arms, in order to clarify the role played by the latter in the coupling forces. The aim of this work is to contribute with the development of novel iodine capture materials through a rationalization of the encapsulation process in metal-containing systems.

COMPUTATIONAL DETAILS

Relativistic density functional theory[34] calculations were carried out by using the ADF code[35], via the scalar ZORA Hamiltonian. An all electron triple-ξ Slater basis set including a polarization function (STO-TZP) was employed within the generalized gradient approximation (GGA) of Becke and Perdew (BP86)[36,37]. The good performance of the BP86 functional has been demonstrated in the study of equilibrium bond lengths of transition-metal diatomic molecules[38], intermolecular hydrogen bonds in a series of sandwich double-decker tetradiazepinoporphyrazine-based lanthanide complexes[39], and in the rationalization of noncovalent interactions of cadmium(II) coordination compounds[40]. Geometry optimizations were conducted via the analytical energy gradient method implemented by Verluis and Ziegler[41]. The Grimme dispersion correction was incorporated in order to properly account for weak London forces[42].

A Noncovalent Interactions Analysis (NCI), as proposed by Yang and coworkers, was conducted by using the NCIPLOT-3.0[28] and NCImilano codes, the later using the electron density from ADF calculations[29]. Furthermore, an Energy Decomposition Analysis was carried out following the Morokuma-Ziegler scheme[30,31], and complemented by a NPA Analysis[32]. Finally, the Atomic Multipole Moment Analysis proposed by Swart and coworkers[33], was used to study in deep the electronic cloud variation at the binding sites and iodine atoms. For all isosurfaces and figures the software packages Chemcraft[43] and Visual Molecular Dynamics (VMD)[44] were used.

RESULTS AND DISCUSSION

The ester-substituted systems subject of this study were recently synthesized by Ura and coworkers[20] via reactions of $[MCl_2(MeCN)_2]$ (M = Pd, Pt) with *m*-$C_6H_4(CMe_2SCH_2CO_2Me)_2$ leading to $[M(\mu\text{-}SCH_2CO_2Me)_2]_8$, hereafter referred as **1**-Pd_8 and **1**-Pt_8. The palladium complex can react with I_2 in $CHCl_3$ at room temperature to generate the inclusion compound **1**-$Pd_8\subset I_2$. To obtain a detailed picture of the noncovalent forces established between the iodine guest and the tiara-like hosts we extend the series also covering the hypothetical systems **1**-Ni_8, **1**-$Ni_8\subset I_2$ and **1**-$Pt_8\subset I_2$. Additionally, we replace the methoxycarbonylmethyl arms by methyl groups (**2**) and hydrogens (**3**) in order to determine the influence of the ester substituents in the iodine encapsulation.

All the ester-substituted complexes can be adjusted to a D_2 symmetry given the ellipsoidal shape of their inner cavity defined by eight metal centers M(II) (M = Ni, Pd, Pt) bridged by sulphur atoms. We label these metal centers as M1, M2 and M3 starting from that contained in the largest symmetry axis of the ellipsoidal cavity. The results are presented in Table 1 and Figure 1. It seems that the inclusion of the iodine guest does not alter in a great extent the size of the cavity as evidenced by the small variation of M···M distances and angles. On the other hand, the typical iodine bond length (2.667 Å)[45] is enlarged to 2.989 Å in **1**-$Ni_8\subset I_2$, 2.903 Å in **1**-$Pd_8\subset I_2$ and 2.880 Å in **1**-$Pt_8\subset I_2$ suggesting that noncovalent interactions occur between the iodine atoms and the M1 centers that could lead to a further dissociation of I_2. The comparison of van der Waals radii sum[46] and M···I distances also suggest that a certain degree of orbital overlap occurs between M1 and the guest, with values of M1···I of 2.879 Å in **1**-$Ni_8\subset I_2$, 3.153 Å

in **1**-Pd_8⊂I_2, and 3.204 Å in **1**-Pt_8⊂I_2, smaller than those corresponding to the van der Waals radii sums (3.220 Å, 3.370 Å and 3.340 Å, respectively). With respect to M2···I, calculated distances are longer than van der Waals radii sums, with the exception of **1**-Ni_8⊂I_2 where a shorter distance is found (3.083 Å), that can be ascribed to stronger interactions. Recently, Devatour-Vinot and coworkers determined by a combining spectroscopic and computational study that I_2 molecules directly interact with the Ni(II) ions of a Ni(pz)[$Ni(CN)_4$] lattice displaying M···I distances of 3.42 Å[9].

DFT calculations at the MPW1PW91/LANL2DZ (Pd), DGDZVP (I), 6-31G (S,H) level were previously carried out by Ura and coworkers for a hypothetical hydrogen-substituted [Pd(μ-$SH)_2]_8$⊂I_2 tiara-like compound providing M···I distances close to those obtained in this work[27].

In order to clarify the role of the metal centers as binding sites and to determine if the sulphur atoms surrounding the I_2 also play a relevant role in keeping the guest in the cavity center, we carried out a Noncovalent Interaction Analysis (NCI)[28,29], which is based on a 2D plot of the reduced density gradient *s*, and the electron density ρ, where *s* can be expressed as

$$s = \frac{1}{2(3\pi^2)^{1/3}} \frac{\nabla\rho}{\rho^{4/3}}$$

When non-covalent interactions occur, there is a crucial change in *s*, producing density critical points. Then, an isosurface considering only those values of *s* associated to the critical points is generated evidencing the regions where noncovalent forces arise. To determine the type of interaction, the second eigenvalue of the electronic density Hessian (λ_2) is invoked, where more than weak stabilizing interactions, such as hydrogen bonds, are characterized by $\lambda_2 < 0$, non-bonded interactions such as steric repulsion by $\lambda_2 > 0$, and weak interactions by $\lambda_2 \approx 0$. These λ_2 values are denoted over the isosurface,

by using a color scale. In the ester-substituted complexes NCI analysis (Figure 2) the blue regions of the isosurface denote that more than weak interactions arise between the metal centers M1 and the iodine atoms. On the other hand, between M2 and the iodine atoms, the intensity of noncovalent interactions seems to be lower, as denoted by the turquish region, while weak London forces between M3 and the iodine molecule are evidenced by the green region of the isosurface suggesting a more important role of M1 in keeping the iodine molecule in the host cavity. The NCI analysis also reveals that sulphur atoms do not interact with I_2 to the same extent as the metal centers.

The nature of the host-guest interactions between the tiara-like host and the iodine guest can be explored in deep through the Energy Decomposition Analysis (EDA) proposed by Morokuma[30,31] which separates the total interaction energy in different terms such as electrostatic, Pauli repulsion, and orbital overlapping, thus clarifying the nature of the interactions arising in several systems[47,48,49,50]. In this analysis, the interaction between the frozen charge densities is accounted by the electrostatic interaction ΔE_{elec}, which is calculated by subtracting the Coulomb integral of the fragments from that corresponding to the overall system. The product of density fragments, which is normalized but violates the Pauli principle, is antisymmetrized and renormalized to give an intermediate state. The energy difference between the states before and after the antisymmetrization-renormalization is called Pauli repulsion, ΔE_{Pauli}, and can be related to destabilizing forces between the fragments. Finally, the fragment orbitals are relaxed to yield the final state corresponding to the inclusion system. The energy decrease caused from such orbital mixing is identified as the orbital interaction, ΔE_{orb}. Adding ΔE_{elec}, ΔE_{Pauli}, and ΔE_{orb} we obtain the total interaction energy ΔE_{int}, of the fragments. To overcome the basis set superposition error (BSSE), the counterpoise method proposed by Boys and Bernardi is employed[51], denoting in this case BSSE values of about 4.15 kcal mol^{-1}. The

dispersion interaction is included according to the Grimme pairwise dispersion correction[42] where an attractive energy term summed over all atomic pairs is incorporated, taking into account the weak forces associated to instantaneous fluctuations of fragment electronic densities. Finally, the energy difference between the initial geometries of the fragments and those belonging to the inclusion systems is denoted as preparation energy, ΔE_{prep}.

The EDA results presented in Table 2 reveals that in the ester-substituted series, all systems present almost the same total interaction energy, with values of -56.61 kcal mol^{-1} for **1**-$Ni_8\subset I_2$, -60.34 kcal mol^{-1} for **1**-$Pd_8\subset I_2$, and -58.73 kcal mol^{-1} for **1**-$Pt_8\subset I_2$, indicating that there is not a clear preference of iodine for a particular tiara-like compound. Looking for the main contribution to stabilizing forces, the electrostatic contribution arises in the three inclusion compounds as the most important (~ 45%) followed by orbital contribution (~ 32%) and dispersion energy (~ 23%).

The EDA analysis for the ester-substituted systems also indicates that the highest preparation energy is obtained for **1**-$Pt_8\subset I_2$ (350.43 kcal mol^{-1}) denoting that more pronounced structural variations occur with the encapsulation of the guest in this case. The orbital contribution in **1**-$Ni_8\subset I_2$ (-95.44) evidences a higher extent of orbital overlap for this complex probably due to the smaller M···I distances. This higher orbital contribution in **1**-$Ni_8\subset I_2$ allows a more effective charge transfer during the inclusion process as is reflected in the NPA results (See discussion below). On the other hand, the electrostatic contribution increases as the metal centers of the tiara-like host present more localized orbitals being -72.04 kcal mol^{-1} for **1**-$Pt_8\subset I_2$, -73.89 kcal mol^{-1} for **1**-$Pd_8\subset I_2$, and -131.38 kcal mol^{-1} for **1**-$Ni_8\subset I_2$.

The dispersion energy according to the Grimme correction[42] increases in line with the volume of the metal binding sites with values of -37.80 kcal mol^{-1} in **1**-$Ni_8\subset I_2$, -47.62 kcal mol^{-1} in **1**-$Pd_8\subset I_2$, and -49.28 kcal mol^{-1} in **1**-$Pt_8\subset I_2$. The opposite occurs with the Pauli term accounting for repulsion forces, that reaches its maximum value in **1**-$Ni_8\subset I_2$, a fact that could be attributed to the shorter M···I distances that enhance the steric repulsions.

The replacement of the alternately located methoxycarbonylmethyl arms by methyl groups leads to a decrease in preparation energy, which now ranges from 128.66 kcal mol^{-1} in **2**-$Ni_8\subset I_2$ to 161.70 kcal mol^{-1} in **2**-$Pt_8\subset I_2$, suggesting that structural variations occurring in **1** could be associated to the ester arms rearrangements. The subsequent replacement of methyl substituents by hydrogens results in a more pronounced decrease of such energy now ranging from 75.28 kcal mol^{-1} in **3**-$Ni_8\subset I_2$ to 79.78 kcal mol^{-1} in **3**-$Pt_8\subset I_2$. Conversely, the replacement of the ester arms does not influence significantly the orbital and electrostatic contributions. The same occurs with the Pauli term where the incorporation of the methyl groups exerts a small influence. However, when we go towards the hydrogen-substituted complexes, a steep decrease of Pauli repulsion occurs, now ranging from 190.37 kcal mol^{-1} in **3**-$Ni_8\subset I_2$ to 98.22 kcal mol^{-1} in **3**-$Pt_8\subset I_2$. These results indicate that steric effects in the ester-substituted series can be mainly attributed to the methylene groups attached to the sulphur atoms.

The nature of the side arms can also affect the host-guest capabilities of the studied structures, by preventing access to the binding sites provided by the M_8 backbone. In this regard, it has been shown earlier by Higgins III and coworkers, that the related [Pd_8(S-*n*Pr)$_{16}$] complex is not able to encapsulate I_2 among other neutral molecules[52], in contrast to results obtained with **1**-Pd_8, by Ura and coworkers[20]. This reflects that variation of

steric effects related to the ligands could also be a good strategy towards a fine tuning of host capabilities provided by the multimetallic array.

Looking for a deeper understanding of the electrostatic contribution to total interaction energy, we study the electronic cloud distortion experienced by the metal centers in terms of dipole moments and quadrupole moments, according to the methodology proposed by Swart and coworkers[33] where the local electrostatic potential is mainly determined by the charge distribution around the respective atom, or within the atomic multipole expansion, by the atomic multipoles near to that point. This charge analysis offers an accurate description of the electrostatic potential from the charge distribution in molecules by writing the total density as a sum of atomic densities expressed in terms of atomic functions, which in turn are used to define a set of atomic multipoles. The results of the atomic multipole analysis are presented in Table 4, where it is clear that before the iodine molecule inclusion, the dipole moments of the metal centers exhibit an almost negligible distortion, as reflected by values under 0.12 D that can be attributed to their slightly distorted square planar coordination sphere. With the incorporation of I_2 a noticeable variation of the metal centers dipoles is observed, especially in the M1 centers. Thus, in **1**-$Pd_8\subset I_2$ the M1 dipole reaches its highest value of 0.737 D, followed by 0.344 D in **1**-$Ni_8\subset I_2$ and 0.260 D in **1**-$Pt_8\subset I_2$, well above to those observed for M2 and M3. A correspondence between the magnitude of M1 dipoles and those related to the iodine atoms is observed, although with lower magnitudes for the later ones, i.e. 0.223 D in **1**-$Pd_8\subset I_2$, 0.177 D in **1**-$Pt_8\subset I_2$, and 0.150 D in **1**-$Ni_8\subset I_2$. The graphical representation of the atomic dipoles also evidences the proper head-to-tail orientation for the M1 and iodine dipoles leading to the dipole-dipole forces (Figure 3), also present in the methyl-substituted and hydrogen substituted series (Figure S1).

In the methyl-substituted (**2**) and hydrogen-substituted (**3**) series, we can also observe low magnitude electronic dipoles for the metal centers before the guest encapsulation, where only the platinum centers of the hydrogen-substituted series overcome the barrier of 0.12 D. In almost all cases, the guest incorporation leads to electronic rearrangements in which M1 presents the highest dipole value, with the exception of **2**-$Pt_8\subset I_2$ and **3**-$Pt_8\subset I_2$ where M2 centers exhibit the maximum dipole moments of 0.132 D and 0.131 D, respectively.

In addition to dipole-dipole forces, the quadrupole-quadrupole interactions also play a relevant role in electrostatic forces. Bearing this in mind, we calculate the atomic quadrupole tensors for the metal centers and the iodine atoms. Then, we determine the anisotropy of such tensors in order to quantify the degree of electronic cloud distribution. Also we plot the quadrupole tensors in order to acquire a deeper knowledge in the electronic rearrangement occurring at the binding sites with the I_2 incorporation. Results are presented in Table 5.

In the ester-substituted series the quadrupole anisotropy is more pronounced for the M2 centers with values of -7.721 B for **1**-$Pd_8\subset I_2$, -5.910 B for **1**-$Pt_8\subset I_2$ and 1.025 B for **1**-$Ni_8\subset I_2$. On the other hand, the iodine atoms experience a quadrupole distortion in line with that observed in the dipoles case, with the maximum anisotropy value of 4.212 B for **1**-$Pd_8\subset I_2$, followed by 4.062 B for **1**-$Pt_8\subset I_2$, and 3.335 B for **1**-$Ni_8\subset I_2$.

The graphical representation of the quadrupole moment tensors allows us to notice that a different distribution is obtained in **1**-$Ni_8\subset I_2$, where the positive lobes of the metal centers point towards the center of the cavity avoiding the opposite-sign interaction with the negative lobe of the iodine quadrupole. Conversely, in **1**-$Pd_8\subset I_2$ and **1**-$Pt_8\subset I_2$ the metal negative lobes point towards the center of the cavity leading to an effective match

between the negative lobe of M1 and the iodine positive lobe. Also, this distribution allows a closer distance between M2 negative lobes and iodine positive lobes in good agreement with the higher M2 quadrupole anisotropy values found for the palladium and platinum systems. The same quadrupole distributions are obtained with the methyl-substituted (**2**) and hydrogen-substituted systems (**3**) (Figure S2). Hence, the multipole results evidence a more relevant role played by the dipole-dipole and quadrupole-quadrupole interactions in **1**-$Pd_8{\subset}I_2$ and **1**-$Pt_8{\subset}I_2$ in comparison to **1**-$Ni_8{\subset}I_2$.

A series of hypothetical hydrogen-substituted complexes (**3**) enables us to carry out a Natural Population Analysis to obtain a deeper understanding of the charge transfer occurring during the guest inclusion. The optimized structures of **3** present M···I distances in good agreement to those corresponding to the ester-substituted frameworks (Table S1). The NPA results presented in Table 3 suggest that an electronic charge transfer from the metal centers to the iodine guest occurs, which is more pronounced in **3**-$Ni_8{\subset}I_2$ -in line with the higher orbital contribution obtained in the EDA- with an average charge of +0.40 |e| for each metal center and an overall charge of -1.14 |e| for I_2. In $Pd_8{\subset}I_2$ and $Pt_8{\subset}I_2$ the electronic transfer leads to lower M charges of +0.30 |e| and +0.19 |e|, respectively and an overall charge of -0.70 |e| for I_2 in both cases. The NPA analysis also evidences that sulphur atoms do not experience an important charge transfer with the guest incorporation.

CONCLUDING REMARKS

The Energy Decomposition Analysis reveals that **1**-Ni_8, **1**-Pd_8 and **1**-Pt_8 thiolate complexes are capable to establish noncovalent interactions with the iodine molecule to a similar extent as evidenced by the total interaction energies of their corresponding inclusion systems (-56.61 kcal mol^{-1}, -60.34 kcal mol^{-1}, and -58.73 kcal mol^{-1}, respectively). In all of them, the electrostatic contribution arises as the most important term representing about 45% of total interaction, a remarkable feature considering the formally neutral character of both the host and the guest. The nickel system presents the higher orbital contribution in line with a major amount of charge transferred during the encapsulation process. Interestingly, a rise of multipole-multipole forces occur in **1**-$Pd_8 \subset I_2$ and **1**-$Pt_8 \subset I_2$, as revealed by the higher electronic cloud deviation experienced by the metal centers, in terms of dipole magnitudes (M1) and quadrupole anisotropies (M2). Moreover, a correspondence between the electronic cloud deformation degree of the metal centers and that concerning the iodine atoms is found.

The studied systems constitute promising iodine sequestering agents. Thus, our results shed light into the interesting application of the nickel tiara-like host [Ni(μ-$SCH_2CO_2Me)_2]_8$ as an alternative to the reported [Pd(μ-$SCH_2CO_2Me)_2]_8$ complex. This can

be useful for further evaluation of nickel-based iodine encapsulating systems prior to engaging in explorative synthesis efforts.

ACKNOWLEDGEMENTS

The authors thank the financial support from FONDECYT 1140359 and MILLENNIUM PROJECT RC120001 grants.

TABLES AND FIGURES

Table 1: Selected structural parameters of the studied systems (Å and degrees).

	1-Ni_8	**1**-$Ni_8 \subset I_2$	**1**-Pd_8		**1**-$Pd_8 \subset I_2$		**1**-Pt_8		**1**-$Pt_8 \subset I_2$
			Exp.[a]	Theor.	Exp.[a]	Theor.	Exp.[b]	Theor.	
M1···M1	8.612	8.747	8.719	9.051	-	9.209	8.754	9.049	9.288
M2···M2	8.002	8.085	8.233	8.677	-	8.753	8.801	8.812	8.908
M3···M3	7.332	7.396	8.231	8.307	-	7.924	8.434	8.518	8.083
< M2-M1-M2	121.2	126.7	131.3	130.2	-	130.1	134.7	132.1	131.1
< M1-M2-M3	134.8	135.3	133.9	135.1	-	132.2	136.2	134.6	131.7
< M2-M3-M2	143.1	142.6	136.4	139.6	-	145.3	137.0	138.8	145.4
M1···I	-	2.879	-	-	3.099	3.153	-	-	3.204
M2···I	-	3.083	-	-	3.402	3.449	-	-	3.536
M3···I	-	3.989	-	-	4.198	4.219	-	-	4.291
I-I	-	2.989	-	-	2.762	2.903	-	-	2.880

a. Experimental data from reference 27
b. Experimental data from reference 15

Table 2: Energy Decomposition Analysis (EDA) (kcal mol^{-1}) for the octanuclear tiara-like complexes.

	1-$Ni_8 \subset I_2$		**1**-$Pd_8 \subset I_2$		**1**-$Pt_8 \subset I_2$	
ΔE_{prep}	301.69		308.54		350.43	
ΔE_{orb}	-95.44	36.07%	-53.09	30.41%	-50.68	29.47%
ΔE_{elec}	-131.38	49.65%	-73.89	42.32%	-72.04	41.88%
ΔE_{disp}	-37.80	14.28%	-47.62	27.27%	-49.28	28.65%
ΔE_{Pauli}	208.01		114.26		113.27	
ΔE_{int}	-56.61		-60.34		-58.73	
	2-$Ni_8 \subset I_2$		**2**-$Pd_8 \subset I_2$		**2**-$Pt_8 \subset I_2$	
ΔE_{prep}	128.66		130.15		161.70	
ΔE_{orb}	-97.32	36.58%	-54.32	30.77%	-51.44	29.80%
ΔE_{elec}	-132.81	49.91%	-76.60	43.39%	-73.96	42.84%
ΔE_{disp}	-35.95	13.51%	-45.62	25.84%	-47.24	27.36%
ΔE_{Pauli}	206.66		117.35		115.43	
ΔE_{int}	-59.42		-59.19		-57.21	
	3-$Ni_8 \subset I_2$		**3**-$Pd_8 \subset I_2$		**3**-$Pt_8 \subset I_2$	
ΔE_{prep}	75.28		65.89		79.78	
ΔE_{orb}	-81.21	35.42%	-41.38	27.59%	-39.30	27.46%
ΔE_{elec}	-120.00	52.34%	-69.41	46.28%	-63.31	44.23%
ΔE_{disp}	-28.06	12.24%	-39.18	26.13%	-40.53	28.31%
ΔE_{Pauli}	190.37		105.29		98.22	
ΔE_{int}	-38.90		-44.68		-44.92	

Table 3. Natural population analysis (NPA, a.u.) of the hydrogen-substituted metallacycle complexes. M1 corresponds to the metal center closest to an iodine atom.

	3-Ni_8	**3**-$Ni_8 \subset I_2$	**3**-Pd_8	**3**-$Pd_8 \subset I_2$	**3**-Pt_8	**3**-$Pt_8 \subset I_2$
M 1	0.35	0.41	0.29	0.31	0.17	0.20
M 2	0.35	0.40	0.29	0.31	0.17	0.19
M 3	0.35	0.38	0.29	0.29	0.17	0.17
I	-	-0.57	-	-0.35	-	-0.35
S 1 (H in)	-0.33	-0.32	-0.29	-0.28	-0.24	-0.23
S 1 (H out)	-0.33	-0.31	-0.29	-0.28	-0.24	-0.23
S 2 (H in)	-0.33	-0.32	-0.29	-0.28	-0.24	-0.22
S 2 (H out)	-0.33	-0.32	-0.29	-0.29	-0.24	-0.24

Table 4: Electronic dipole vectors for metal and guest atoms (Debyes). M1 corresponds to the metal center closest to an iodine atom.

	1-Ni_8	**1**-$Ni_8{\subset}I_2$	**1**-Pd_8	**1**-$Pd_8{\subset}I_2$	**1**-Pt_8	**1**-$Pt_8{\subset}I_2$
M1	0.114	0.344	0.007	0.737	0.046	0.260
M2	0.047	0.046	0.031	0.056	0.068	0.091
M3	0.076	0.100	0.010	0.220	0.039	0.001
I	-	0.150	-	0.223	-	0.177
	2-Ni_8	**2**-$Ni_8{\subset}I_2$	**2**-Pd_8	**2**-$Pd_8{\subset}I_2$	**2**-Pt_8	**2**-$Pt_8{\subset}I_2$
M1	0.006	0.206	0.041	0.309	0.110	0.121
M2	0.006	0.019	0.041	0.028	0.110	0.132
M3	0.006	0.023	0.041	0.060	0.110	0.108
I	-	0.153	-	0.270	-	0.193
	3-Ni_8	**3**-$Ni_8{\subset}I_2$	**3**-Pd_8	**3**-$Pd_8{\subset}I_2$	**3**-Pt_8	**3**-$Pt_8{\subset}I_2$
M1	0.019	0.229	0.059	0.279	0.136	0.085
M2	0.016	0.020	0.059	0.042	0.133	0.131
M3	0.015	0.036	0.059	0.044	0.128	0.127
I	-	0.137	-	0.220	-	0.114

Table 5. Anisotropy of the electronic quadrupole tensors for the representative metal and guest atoms (Buckinghams). M1 corresponds to the metal center aligned with the iodine molecule.

	1-Ni_8	**1**-$Ni_8 \subset I_2$	**1**-Pd_8	**1**-$Pd_8 \subset I_2$	**1**-Pt_8	**1**-$Pt_8 \subset I_2$
M 1	0.630	0.744	-3.701	-3.362	-3.002	-2.943
M 2	1.016	1.025	-7.203	-7.721	-5.591	-5.910
M 3	0.750	0.791	-3.635	3.023	-3.028	-3.063
I	-	3.335	-	4.212	-	4.062
	2-Ni_8	**2**-$Ni_8 \subset I_2$	**2**-Pd_8	**2**-$Pd_8 \subset I_2$	**2**-Pt_8	**2**-$Pt_8 \subset I_2$
M 1	0.543	0.593	-3.780	-4.054	-3.302	-3.187
M 2	0.851	0.855	-6.546	-6.778	-5.902	-6.041
M 3	0.543	0.628	-3.780	-3.900	-3.302	-3.455
I	-	3.162	-	4.268	-	4.110
	3-Ni_8	**3**-$Ni_8 \subset I_2$	**3**-Pd_8	**3**-$Pd_8 \subset I_2$	**3**-Pt_8	**3**-$Pt_8 \subset I_2$
M 1	0.678	0.681	-3.192	-3.777	-2.945	-3.003
M 2	1.107	1.017	-5.379	-6.058	-5.220	-5.549
M 3	0.687	0.756	-3.186	-3.527	-2.958	-3.123
I	-	3.584	-	4.319	-	4.283

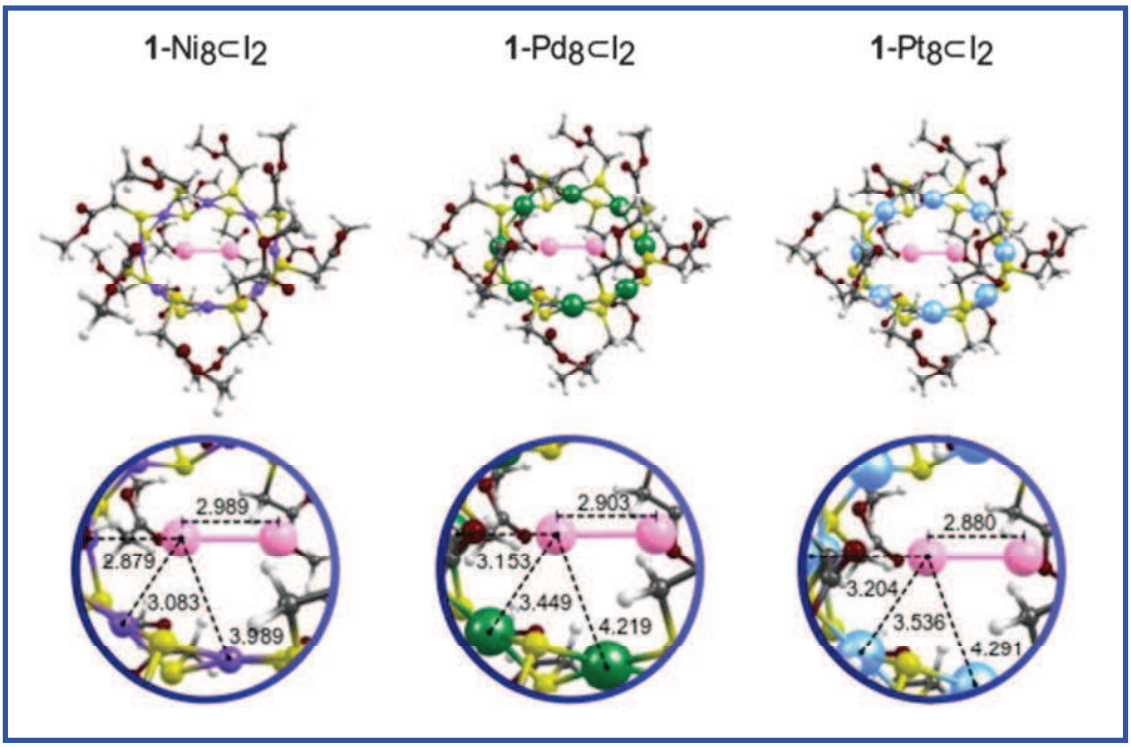

Figure 1. Optimized geometries of the inclusion compounds (distances in Å)

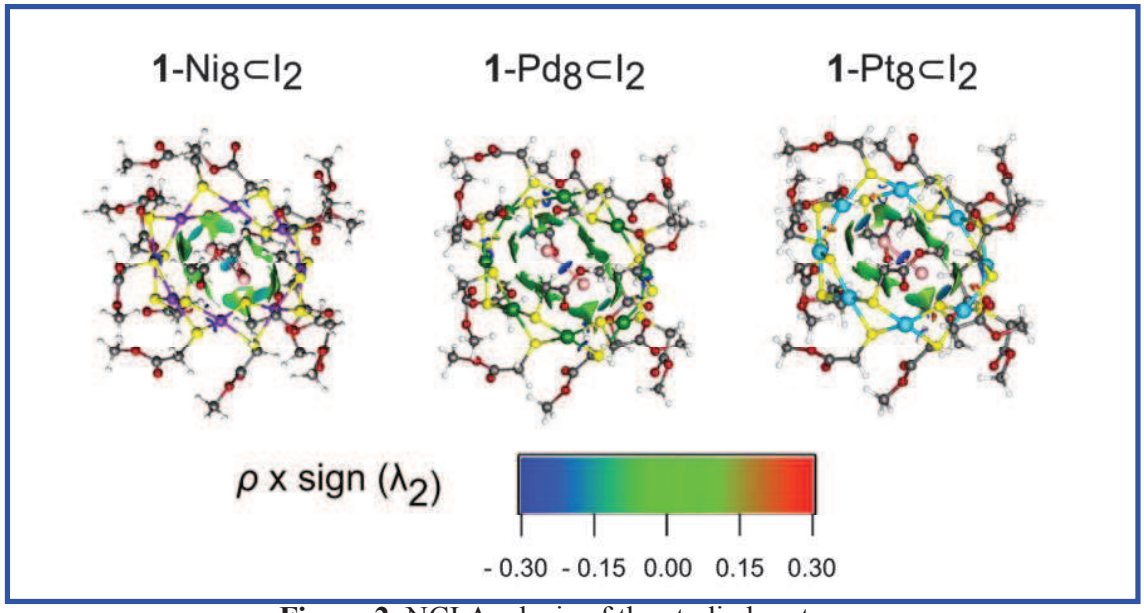

Figure 2. NCI Analysis of the studied systems.

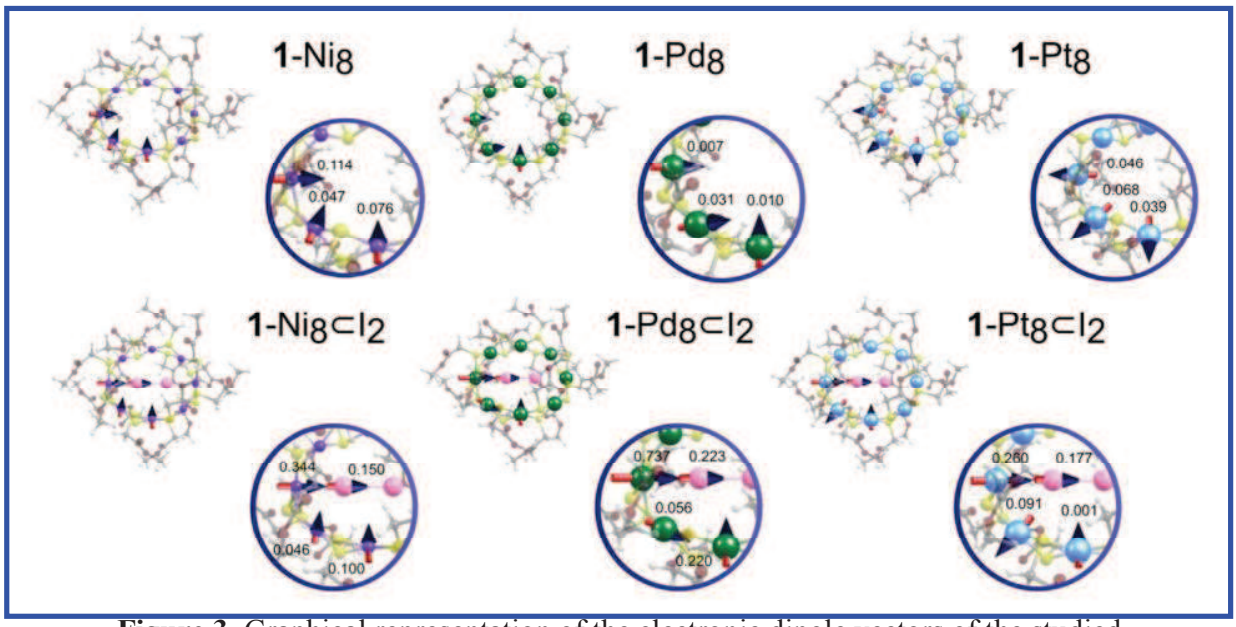

Figure 3. Graphical representation of the electronic dipole vectors of the studied systems where the blue arrowhead denotes the negative region (Debyes).

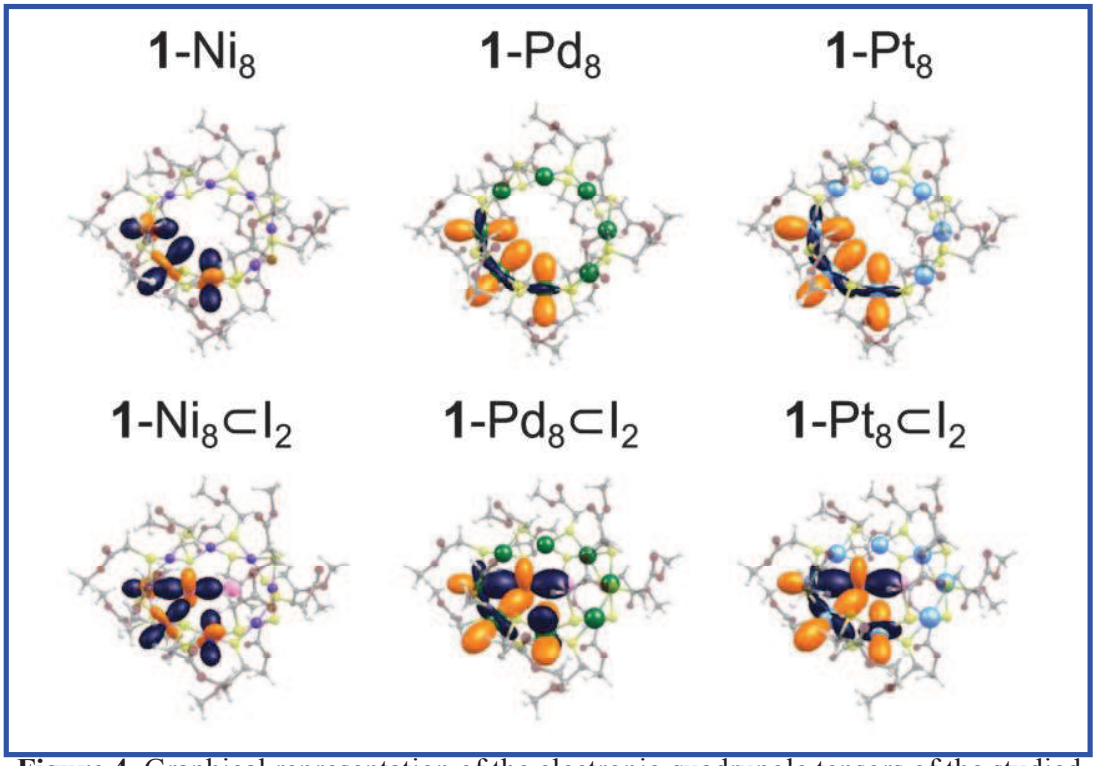

Figure 4. Graphical representation of the electronic quadrupole tensors of the studied systems (orange lobes denote negative regions and the blue ones, positive regions).

SUPPORTING INFORMATION AVAILABLE

Selected calculated distances (Å) and angles (degrees), graphical representation of the dipole vectors, and graphical representation of the quadrupole moments tensors for the methyl-substituted (**2**) and the hydrogen-substituted (**3**) series are available free of charge at http://pubs.acs.org.

BIBLIOGRAPHIC REFERENCES

[1] Chapman, K. W.; Chupas, P. J.; Nenoff, T. M. Radioactive Iodine Capture in Silver-Containing Mordenites through Nanoscale Silver Iodide Formation. *J. Am. Chem. Soc.* **2010**, *132*, 8897-8899.

[2] Sava, D. F.; Rodriguez, M. A.; Chapman, K. W.; Chupas, P. J.; Greathouse, J. A.; Crozier, P. S.; Nenoff, T. M. Capture of Volatile Iodine, a Gaseous Fission Product, by Zeolitic Imidazolate Framework-8. *J. Am. Chem. Soc.* **2011**, *133*, 12398-12401.

[3] Sava, D. F.; Garino, T. J.; Nenoff, T. M. Iodine Confinement into Metal-Organic Frameworks (MOFs): Low-Temperature Sintering Glasses to form Novel Glass Composite Material (GCM) Alternative Waste Forms. *Ind. Eng. Chem. Res.* **2012**, *51*, 614-620.

[4] Riley, B. J.; Vienna, J. D.; Strachan, D. M.; McCloy, J. S.; Jerden, J. L. Jr. Materials and Processes for the Effective Capture and Immobilization of Radioiodine: A Review. *J. Nucl. Mater.* **2016**, *470*, 307-326.

[5] Hu, J.; Wang, D.; Guo, W.; Du, S.; Tang, Z. K. Reversible Control of the Orientation of Iodine Molecules inside the $AlPO_4$-11 Crystals. *J. Phys. Chem. C* **2012**, *116*, 4423-4430.

[6] Bronić, J.; Sekovanić, L.; Mužic, A.; Biljan, T.; Kontrec, J.; Subotić, B. Host-Guest Interaction of Iodine with Zeolite A. *Acta Chim. Slov.* **2006**, *53*, 166-171.

[7] Rachuri, Y.; Bisht, K. K.; Suresh, E. Two-Dimensional Coordination Polymers Comprising Mixed Tripodal Ligands for Selective Colorimetric Detection of Water and Iodine Capture. *Crystal Growth & Design* **2014**, *14*, 3300-3308.

[8] Massasso, G.; Long, J.; Guerin, C.; Grandjean, A.; Onida, B.; Guari, Y.; Larionova, J.; Maurin, G.; Devautour-Vinot, S. Understanding the Host/Guest Interactions in Iodine/Hoffmann-Type Clathrate Ni(pz)[$Ni(CN)_4$] System. *J. Phys. Chem C* **2015**, *119*, 9395-9401.

[9] Arıcı, M; Yeşilel, O. Z.; Taş, M.; Demiral, H. Effect of Solvent Molecule in Pore for Flexible Porous Coordination Polymer upon Gas Adsorption and Iodine Encapsulation. *Inorg. Chem.* **2015**, *54*, 11283-11291.

[10] Ma, S.; Islam, S. M.; Shim, Y.; Gu, Q.; Wang, P.; Li, H.; Sun, G.; Yang, X.; Kanatzidis, M. G. Highly Efficient Iodine Capture by Layered Double Hydroxides Intercalated with Polysulfides. *Chem. Mater.*, **2014**, *26*, 7114-7123.

[11] Falaise, C.; Volkringer, C.; Facqueur, J.; Bousquet, T.; Gasnot, L.; Loiseau, T. Capture of Iodine in Highly Stable Metal-Organic Frameworks: A Systematic Study. *Chem. Commun.* **2013**, *49*, 10320-10322.

[12] Rama, T.; Alvariño, C.; Domarco, O.; Platas-Iglesias, C.; Blanco, V.; García, M. D.; Peinador, C.; Quintela, J. M. Self-assembly of Pd_2L_2 Metallacycles Owning Diversely Functionalized Racemic Ligands. *Inorg. Chem.* **2016**, *55*, 2290-2298.

[13] Fan, Q.-J.; Zhang, W.-Y.; Lin, Y.-J.; Jin, G.-X. Construction of Tetranuclear Metallacycles based on Half-Sandwich Ir, Rh fragments and Pyridyl-substituted Ligands with Different Coordinate Vectors. *Dalton Trans.* **2016**, *45*, 4534-4540.

[14] Mezei, G.; Zaleski, C. M.; Pecoraro, V. L. Structural and Functional Evolution of Metallacrowns. *Chem. Rev.* **2007**, *107*, 4933-5003.

[15] Yamashina, Y.; Kataoka, Y.; Ura, Y. Tiara-like Octanuclear Palladium(II) and Platinum(II) Thiolates and their Inclusion Complexes with Dihalo- or Iodoalkanes. *Inorg. Chem.* **2014**, *53*, 3558-3567.

[16] Mohamed, A. A.; Ricci, S.; Burini, A.; Galassi, R.; Santini, C.; Chiarella, G. M.; Melgarejo, D. Y.; Fackler, J. P. Halide and Nitrite Recognizing Hexanuclear Metallacycle Copper(II) Pyrazolates. *Inorg. Chem.* **2011**, *50*, 1014-1020.

[17] Zeng, M.-H.; Wang, Q.-X.; Tan, Y.-X,; Hu, S.; Zhao, H.-X.; Long, L.-S.; Kurmoo, M. Rigid Pillars and Double Walls in a Porous Metal-Organic Framework: Single-

Crystal to Single-Crystal, Controlled Uptake and Release of Iodine and Electrical Conductivity. *J. Am. Chem.* Soc. **2010**, *132*, 2561-2563.

[18] Yu, F.; Li, D.-D.; Cheng, L.; Yin, Z.; Zeng, M.-H.; Porous Supramolecular Networks Constructed of One-Dimensional Metal-Organic Chains: Carbon Dioxide and Iodine Capture. *Inorg. Chem.* **2015**, *54*, 1655-1660.

[19] Duarte, D. J. R.; Sosa, G. L.; Peruchena, N. M.; Alkorta, I. Halogen Bonding. The Role of Polarizability of the Electron-pair Donor. *Phys. Chem. Chem. Phys.* **2016**, *18*, 7300-7309.

[20] Bartashevich, E. V.; Tsirelson, V. G. Atomic Dipole Polarization in Charge-Transfer Complexes with Halogen Bonding. *Phys. Chem. Chem. Phys.* **2013**, 15, 2530-2538.

[21] Volkov, A.; Coppens, P. Calculation of Electrostatic Interaction Energies in Molecular Dimers from Atomic Multipole Moments Obtained by Different Methods of Electron Density Partitioning. *J. Comput. Chem.* **2004**, *25*, 921-934.

[22] Bartashevich, E. V.; Matveychuk, Y. V.; Troitskaya, E. A.; Tsirelson, V. G. Characterizing the Multiple Non-Covalent Interactions in N,S-Heterocycles-diiodine Complexes with focus on Halogen Bonding. *Comput. Theor. Chem.* **2014**, *1037*, 53-62.

[23] Wikfeldt, K. T.; Batista, E. R.; Vila, F. D.; Jónsson, H. A Transferable H_2O Interaction Potential Based on a Single Center Multipole Expansion: SCME. *Phys. Chem. Chem. Phys.* **2013**, *15*, 16542-16556.

[24] Loboda, O.; Ingrosso, F.; Ruiz-López, M. F.; Reis, H.; Millot, C. Dipole and Quadrupole Polarizabilities of the Water Molecule as a Function of Geometry. *J. Comput. Chem.* **2016**, *37*, 2125-2132.

[25] Ponce-Vargas, M.; Muñoz-Castro, A. A Study on the Versatility of Metallacycles in Host–Guest Chemistry: Interactions in Halide-Centered Hexanuclear Copper(II) Pyrazolate Complexes. *Phys. Chem. Chem. Phys*. **2014**, *16*, 13103-13111.

[26] Ponce-Vargas, M.; Muñoz-Castro, A. Heavy Element Metallacycles: Insights into the Nature of Host-Guest Interactions Involving Di-Halide Mercuramacrocycle Complexes. *J. Phys. Chem. C*. **2014**, *118*, 28244-28251.

[27] Yamashina, Y.; Kataoka, Y.; Ura, Y. Inclusion of an Iodine Molecule in a Tiara-Like Octanuclear Palladium Thiolate Complex. *Eur. J. Inorg. Chem.* **2014**, 4073-4078.

[28] Contreras-García, J.; Johnson, E. R.; Keinan, S.; Chaudret, R.; Piquemal, J.; Beratan, D. N.; Yang, W. NCIPLOT: A Program for Plotting Noncovalent Interaction Regions. *J. Chem. Theory Comput.* **2011**, *7*, 625- 632.

[29] Saleh, G., Lo Presti, L., Gatti, C.; Ceresoli, D. NCImilano: An Electron-Density-Based Code for the Study of Noncovalent Interactions. *J. Appl. Cryst.* **2013**, *46*, 1513–1517.

[30] Morokuma, K. Molecular Orbital Studies of Hydrogen Bonds. *J. Chem. Phys.,* **1971**, *55*, 1236-1244.

[31] Su, P.; Li, H. Energy decomposition analysis of covalent bonds and intermolecular interactions. *J. Chem. Phys.* **2009**, *131*, 014102/1-15.

[32] Reed, A. E.; Weinstock, R. B.; Weinhold, F. Natural Population Analysis. *J. Chem. Phys*. **1985**, *83*, 735-746.

[33] Swart, M.; Van Duijnen, P.; Snidjers, J. G. A Charge Analysis Derived from an Atomic Multipole Expansion. *J. Comput. Chem.* **2001**, *22*, 79- 88.

[34] Parr, R.; Yang, W. Density Functional Theory of Atoms and Molecules; Oxford University Press: London, U.K., 1989.

[35] Baerends, E. J.; Ziegler, T.; Autschbach, J.; Bashford, D.; Bérces, A.; Bickelhaupt, F. M.; Bo, C.; Boerrigter, P. M.; Cavallo, L.; Chong, D. P. et al. ADF2014; Vrije Universiteit: Amsterdam, The Netherlands, 2014.

[36] Becke, A. D. Density-functional Exchange Energy Approximation with Correct Asymptotic Behavior. *Phys. Rev. A* **1988**, *38*, 3098-3100.

[37] Perdew, J. P. Density-functional Approximation for the Correlation Energy of the Inhomogeneous Electron Gas. *Phys. Rev. B* **1986**, *33*, 8822-8824.

[38] Barden, C. J.; Rienstra-Kiracofe, J. C.; Schaefer, H. F. Homonuclear 3*d* transition-metal diatomics: A Systematic Density Functional Theory Study. *J. Chem. Phys.* **2000**, *113*, 690-700.

[39] Tarakanova, E. N.; Trashin, S. A.; Simakov, A. O.; Furuyama, T.; Dzuban, A. V.; Inasaridze, L. N.; Tarakanov, P. A.; Troshin, P. A.; Pushkarev, V. E.; Kobayashi, N. et al. Double-decker bis(tetradiazepinoporphyrazinato) Rare Earth Complexes: Crucial Role of Intramolecular Hydrogen Bonding. *Dalton Trans.* **2016**, *45*, 12041-12052.

[40] Banik, R.; Roy, S.; Kirillov, A. M.; Bauza, A.; Frontera, A.; Rodríguez-Diéguez, A.; Salas, J. M.; Maniukiewicz, W.; Das, S. K.; Das, S. Two Mixed-Ligand Cadmium(II) Compounds bearing 5-Nitrosopyrimidine and N-Donor Aromatic Blocks: Self-Assembly Generation, Structural and Topological Features, DFT Studies, and Hirshfeld Surface Analysis. *CrystEngComm* **2016**, *18*, 5647-5657.

[41] Verluis, L.; Ziegler, T. The Determination of Molecular Structures by Density Functional Theory. The Evaluation of Analytical Energy Gradients by Numerical Integration. *J. Chem. Phys.* **1988**, *88*, 322-328.

[42] Grimme, S. Density functional theory with London dispersion corrections. *WIREs Comput. Mol. Sci.* **2011**, *1*, 211-228.

[43] Zhurko, G. A.; Zhurko, D. A. Chemcraft. Version 1.7.

[44] Humphrey, W.; Dalke, A.; Schulten, K. VMD – Visual Molecular Dynamics. *J. Molec. Graph.* **1996**, *14.1*, 33-38.

[45] Hu, J. M.; Zhai, J. P.; Wu, F. M.; Tang, Z. K. Molecular Dynamics Study of the Structures and Dynamics of the Iodine Molecules Confined in $AlPO_4$-11 Crystals. *J. Phys. Chem. B* **2010**, *114*, 16481-16486.

[46] Bondi, A. Van der Waals Volumes and Radii. *J. Phys. Chem.* **1964**, *68*, 441-451.

[47] Hirao, H. Reactive Bond Orbitals: A Localized Resonance-Structure Approach to Charge Transfer. *Chem. Phys. Lett.* **2007**, *443*, 141-146.

[48] Hirao, H. Theoretical Study of Formic Acid: A New Look at the Origin of the Planar Z Conformation and C-O Rotational Barrier. *Chem. Phys.* **2008**, *344*, 213-220.

[49] Hirao, H. Energy Decomposition Analysis of the Protein Environmental Effect: The Case of Cytochrome P450cam Compound I. *Chem. Lett.* **2011**, *40*, 1179-1181.

[50] Hirao, H. The Effects of Protein Environment and Dispersion on the Formation of Ferric-Superoxide Species in *myo*-Inositol Oxygenase (MIOX): A Combined ONIOM(DFT:MM) and Energy Decomposition Analysis. *J. Phys. Chem. B* **2011**, *115*, 11278-11285.

[51] Boys, S. F.; Bernardi, F. The Calculation of Small Molecular Interactions by the Differences of Separate Total Energies. Some Procedures with Reduced Errors. *Mol. Phys.*, **1970**, *19*, 553-566.

[52] Higgins, J. D.; Suggs, J. W. Preparation, Structure and Spectroscopic Studies of the Palladium Mercaptides Pd_8(S-*n*Pr)$_{16}$ and Pd_6(S-*n*Pr)$_{12}$. *Inorg. Chim. Acta*, **1988**, *145*, 247–252.

GRAPHICAL TABLE OF CONTENTS